Non-Ising domain walls in *c*-phase ferroelectric lead titanate thin films

Christian Weymann [ORCID],[1] Salia Cherifi-Hertel [ORCID],[2] Céline Lichtensteiger [ORCID],[1] Iaroslav Gaponenko,[1]
Kokou Dodzi Dorkenoo,[2] Aaron B. Naden [ORCID],[3] and Patrycja Paruch[1]

[1]*Department of Quantum Matter Physics, University of Geneva, 24 Quai Ernest-Ansermet, CH-1211 Geneva 4, Switzerland*
[2]*Université de Strasbourg, CNRS, Institut de Physique et Chimie des Matériaux de Strasbourg, UMR 7504, 67000 Strasbourg, France*
[3]*School of Chemistry, University of St. Andrews, St. Andrews, KY16 9ST, United Kingdom*

Ferroelectrics are technologically important, with wide application in micromechanical systems, nonlinear optics, and information storage. Recent discoveries of exotic polarization textures in these materials, which can strongly influence their properties, have brought to the forefront questions about the nature of their domain walls: long believed to be primarily Ising, with locally null polarization. Here, combining three complementary techniques—second-harmonic generation microscopy, piezoresponse force microscopy, and transmission electron microscopy—to cover all the relevant length scales, we reveal the Néel character (non-Ising polarization oriented perpendicular to the wall) of 180° domain walls in *c*-phase tetragonal ferroelectric lead titanate epitaxial thin films, for both artificial and intrinsic domains at room temperature. Furthermore, we show that variations in the domain density—detected both optically and via local piezoresponse and then quantified by radial autocorrelation analysis—can give us insight into the underlying defect potential present in these materials.

DOI: 10.1103/PhysRevB.106.L241404

Ferroelectric materials are characterized by their spontaneous and reversible electrical polarization, with a wide variety of technological applications as microelectromechanical systems (MEMSs) and memory devices [1]. The electromechanical properties of these materials are closely linked to their domain structure. As such, understanding and controlling the arrangement of domains with different polarization orientation remains a key research objective. In addition, the boundaries between these, i.e., domain walls, can themselves present emergent properties [2–4] potentially attractive for domain-wall-based nanoelectronics [5,6]. Their complex (de)pinning dynamics when driven by an electric field [7] have, in particular, given rise to varied implementations as nanoscale active device components [8,9].

Ferroelectric materials were long believed to present essentially Ising-type 180° domain walls, in which the polarization is maintained along the bulk axis, decreasing to zero and reversing its orientation at the domain wall center. However, extensive theoretical studies [10–16] have predicted non-Ising polarization components oriented either perpendicular to the wall (Néel type) or in the plane of the wall (Bloch type). Previously, the existence of Néel-type domain walls has been demonstrated in Pb(Zr,Ti)O$_3$ [17–19], in addition to the presence of chiral Bloch walls and Bloch lines, a particular type of ferroelectric topological structure, in LiTaO$_3$ [19]. Additional exotic polarization structures, such as arrays of polar vortices [20], "supercrystals" of highly ordered flux closure domains [21–23], and even ferroelectric skyrmions [24,25]

have also recently been reported. In the canonical tetragonal ferroelectric PbTiO$_3$, hosting many of these emergent exotic polarization textures, various theoretical calculations predict either Néel walls [10,26] such as those observed in Pb(Zr$_{0.2}$Ti$_{0.8}$)O$_3$ [18,19], of which it is one of the parent compounds, or a low-temperature Ising-to-Bloch transition at the domains walls [15]. Metastable bubble domains observed in PbTiO$_3$ thin films [27], with no strong delineation between the domain wall and interior, further suggest that the polarization in this material can be extremely "soft" and easy to reorient in either Bloch- or Néel-like textures under specific electrostatic and strain boundary conditions.

In this context, we set out to characterize the nature of 180° domain walls in PbTiO$_3$. Our work is based on three 50-nm PbTiO$_3$ thin films deposited by rf-magnetron sputtering on LaNiO$_3$ electrodes on single-crystal (001) SrTiO$_3$ substrates, with an intrinsic domain configuration governed by the interplay between mechanical and electrostatic boundary conditions [28,29] and additionally controlled via growth temperature defect engineering [30]. Using piezoresponse force microscopy (PFM) and second-harmonic generation (SHG), we find that Néel-like behavior dominates at *artificial* domain walls introduced by local electric field switching of polarization. By combining PFM and careful analysis of transmission electron microscopy (TEM) data, we show that the same is true for *naturally occurring* domain walls in polydomain samples. Finally, we also show that it is possible to extract information on the underlying pinning potential by additional SHG and PFM image treatment and analysis based on autocorrelation.

In the out-of-plane up-oriented monodomain film, domains were patterned by applying relatively high bias to the scanning probe microscopy tip, first +10 V to switch a $6 \times 6\ \mu m^2$ square and then −10 V in a $3 \times 3\ \mu m^2$ square in the center, as shown in Fig. 1(a), ensuring a well-spaced square-in-square
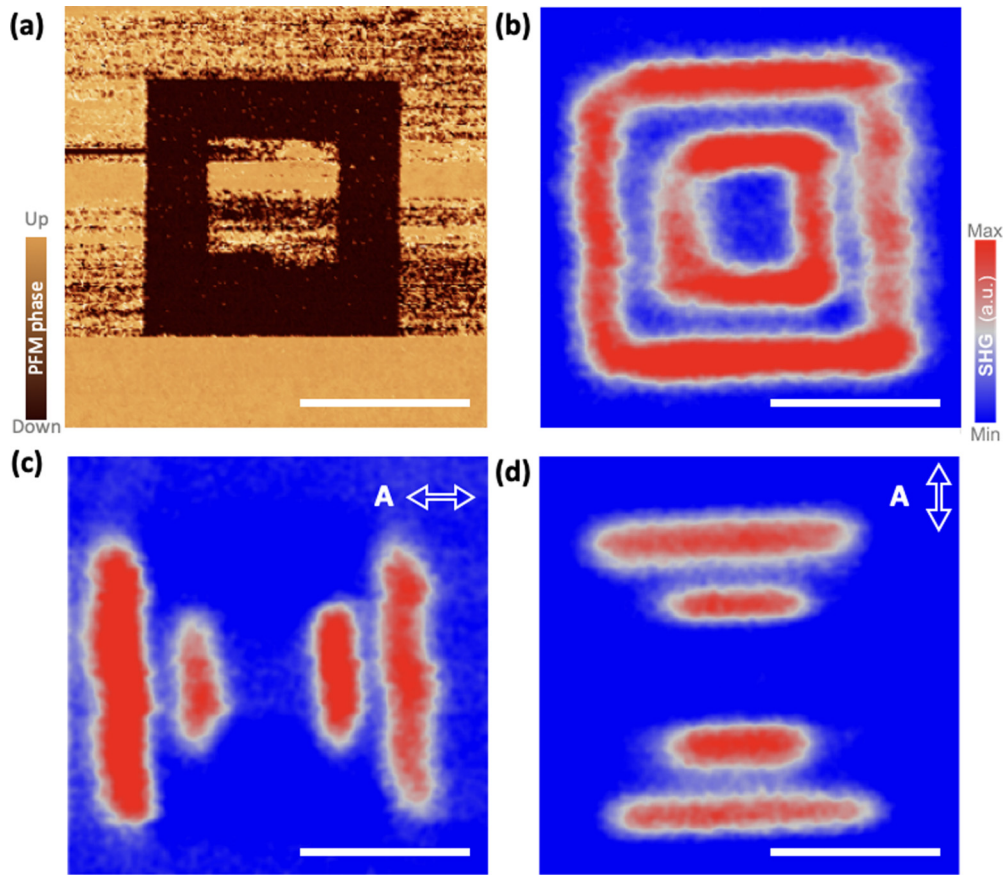
FIG. 1. Signature of Néel polarization at written domain walls at room temperature. (a) Vertical PFM phase image of the square-in-square domain structure written in an up-oriented monodomain film. (b) Isotropic SHG image (without polarization analysis) acquired at the patterned square-in-square domain structure, with red corresponding to maximum signal intensity and blue corresponding to minimum signal intensity. (c) and (d) SHG measurements of the domain structure for different polarizer and analyzer angle combinations, where the analyzer direction is represented by the double-headed arrow. SHG signal is observed at the domain walls only when the analyzer is perpendicular to the domain wall plane, consistent with a Néel character. The white scale bar in all panels represents 4 μm.

domain structure whose walls could be easily individually resolved by SHG. From the anisotropic SHG image [Fig. 1(b)], a localized second-harmonic emission is observed at the domain wall regions, demonstrating their non-Ising polar character. Additional polarimetry analysis was performed on this region for different polarizer and analyzer angle combinations. The written domain walls are clearly visible in the SHG image only when the analyzer is perpendicular to the wall plane, as shown in Figs. 1(c) and 1(d). We can thus conclude that in this case, the domain walls present an in-plane polarization component with a purely Néel-type configuration, as similarly observed in the related material $Pb(Zr_{0.2}Ti_{0.8})O_3$ [19].

For polydomain samples, vertical PFM imaging shows alternating regions with up- and down-oriented domains, of the order of a few tens of nanometers across, as can be seen in Fig. 2(a). At these length scales it impossible to individually resolve domain walls and determine their nature via SHG polarimetry, but non-negligible contrasts in the measured intensity point to the presence of in-plane polarization (as we will discuss further later). We therefore turn to scanning transmission electron microscopy (STEM) to visualize the individual atomic displacements contributing to the macroscopic polarization. TEM measurements were performed on

an ≈30 nm lamella prepared with the long axis parallel to the [100] in-plane axis of the thin film, as schematically indicated by the green box in Fig. 2(a). Capturing a domain wall perfectly edge-on in such a lamella is unlikely, and we thus expect to observe a projection of the wall, in which case the TEM measurements would average over the two opposing out-of-plane polarization orientations of the domains as well as any Néel or Bloch domain wall polarization, as schematically indicated in Figs. 2(b) and 2(c), respectively.

Figure 3(a) shows a low-magnification differential phase contrast (DPC) STEM image where the color scale indicates the direction and relative magnitude of the deflection of the STEM probe due to diffraction and Lorentz deflection. Within the $PbTiO_3$ film, elongated linear features between regions of relatively homogeneous contrast can be identified, appearing dark red and thus indicating an increased in-plane deflection component. These features appear narrower and vertically oriented near the film surface and then gradually broaden and curve towards the interface of the film with the back electrode and substrate. We therefore focused on the near-surface region, to enhance the probability of their edge-on alignment. The red box demarcates an area imaged at atomic resolution in the high-angle annular dark-field (HAADF) image in Fig. 3(b). Here, the abrupt feature in the center can be seen to
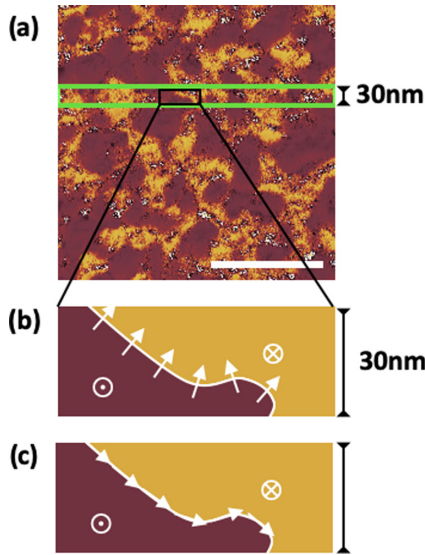
FIG. 2. Top view of nanoscale domains and domain walls. (a) Vertical PFM phase image of the domain structure of a polydomain sample. The white scale bar represents 400 nm. The typical thickness of the TEM lamella prepared from this sample ($\approx$30 nm) is represented by the green box. (b) and (c) Schematic representation of the polarization in the black rectangle in (a), for the case of Néel- (b) or Bloch-type (c) domain walls, respectively. From this schematic representation, it is clear that domain walls are highly unlikely to align through the TEM lamella thickness, but will rather meander, leading to averaging over different polarization orientations in the TEM cross-section measurements. For a wall that is not imaged edge-on, i.e., orthogonal to the plane of the lamella, the two possible polarization configurations at the wall [(b) and (c)] could lead to similar projections.

manifest as a distinct shift in the Pb atom positions, resulting in an apparent "kink" in the Pb lattice (the brightest atom columns). This confirms the prediction of Aguado-Puente and Junquera for 180° domain walls in PbTiO$_3$ thin films [31] and is very similar to the Bi-lattice kink observed in BiFeO$_3$ related to the polarization rotation and accumulation of charged defects at domains walls [32]. Furthermore, it can be seen from Fig. 3(b) and its cropped version shown in Fig. 3(c) that the Ti atom columns sit closer to the center of the unit cell on the left whereas they are near the bottom of the unit cell on the right. In other words, there is evidently a greater out-of-plane component of polarization on the right since this is closely linked to the B-site cation displacement from the centrosymmetric position within the unit cell [33]. This observation therefore suggests the presence of a domain wall in the center of the image.

In order to accurately determine the atom positions and hence polarization, we perform two-dimensional (2D) Gaussian fitting to the Pb and Ti atom columns which offers subpixel precision [34–36]. From this, we can determine a number of factors that can confirm the presence of a domain wall: the *c*-axis *d* spacing and the *c-a* angle (the angle between the [100] and [001] directions), as shown in the averaged line profiles in Fig. 3(d), which go from left to right in Fig. 3(b). In addition, we can also determine the ellipticity of the atom columns—shown in Fig. 3(e)—which gives a measure of the

disorder through the thickness of the lamella: An ideally ordered column of atoms would appear perfectly circular. From the profiles in Figs. 3(d) and 3(e), it is clear that the kink observed in Figs. 3(b) and 3(c) coincides with an increase in the *c-a* angle and in both the Pb and Ti ellipticities. One can also note a concomitant decrease in out-of-plane lattice parameter *c*, although within the error bars. Crucially, all of this occurs over approximately two to three unit cells and coincides with an increase in the in-plane component of the polarization defined by the displacement of the Ti columns from the center of the unit cell given by the Pb atoms, as shown in Fig. 3(e).

To deconvolute the different domain contributions, we fit three 2D Gaussians to each of the Ti atom columns: two corresponding to the Ti atom shifts up and down relative to the mean position given by the single Gaussian fitting and one corresponding to the "mean" position between the first two. This approach is analogous to the MPFIT algorithm proposed previously [37]. We can then reconstruct the dominant polarization from these three components, discarding extraneous effects from projection. We note, however, that the displacement of the Ti atoms only corresponds exactly to the polarization of the PbTiO$_3$ if the Born effective charge is constant, which may not be the case at the domain wall. For the sake of brevity, a comprehensive discussion of the procedure is detailed in Supplemental Material [38] Sec. S1. Figure 3(f) shows the final result of this reconstruction where the image is an interpolated map of the *c-a* angle with the polarization vectors overlaid. Moving from left to right on the image, a classic Néel-like behavior is observed: The polarization rotates through 180° from upwards on the left to downwards on the right with a predominantly in-plane orientation in the two to three unit cells at the Pb kink in the center where the *c-a* angle is maximized and the tetragonality is minimized.

It therefore appears that in our PbTiO$_3$ thin films, at room temperature, both written and intrinsic domain walls present a Néel character. For the written domain walls, tip-related interactions, e.g., electrochemical alteration of the surface [39], could stabilize the polar discontinuity inherent in the Néel structure. For intrinsic domain walls, however, first-principles calculations predict a Bloch character at low temperature and, at higher temperatures, an Ising character with no in-plane component of polarization [15]. Our observations of a Néel component suggest that in real materials such structures are on the contrary at the very least metastable. The polarization discontinuity at domain walls with such a Néel component can be related to domain wall curvature or inclination [40]. Such charged structures, including head-to-head or tail-to-tail polarization [41], could contribute to a higher conductivity at the domain walls [42–46].

Moreover, defects and disorder are a crucial element of ferroelectric thin films, acting as nucleation sites during switching [47], pinning domain walls [7,48,49], and segregating along them to provide a path for electrical conduction [3,50,51]. Further insight into the defect landscape can be obtained from a comparative analysis of PFM and SHG measurements in another polydomain sample (Fig. 4). The vertical PFM phase response in Fig. 4(a) reveals intrinsic domains of the order of 100 nm, well below the diffraction limit for the wavelength used in SHG measurements ($\sim$300 nm). When
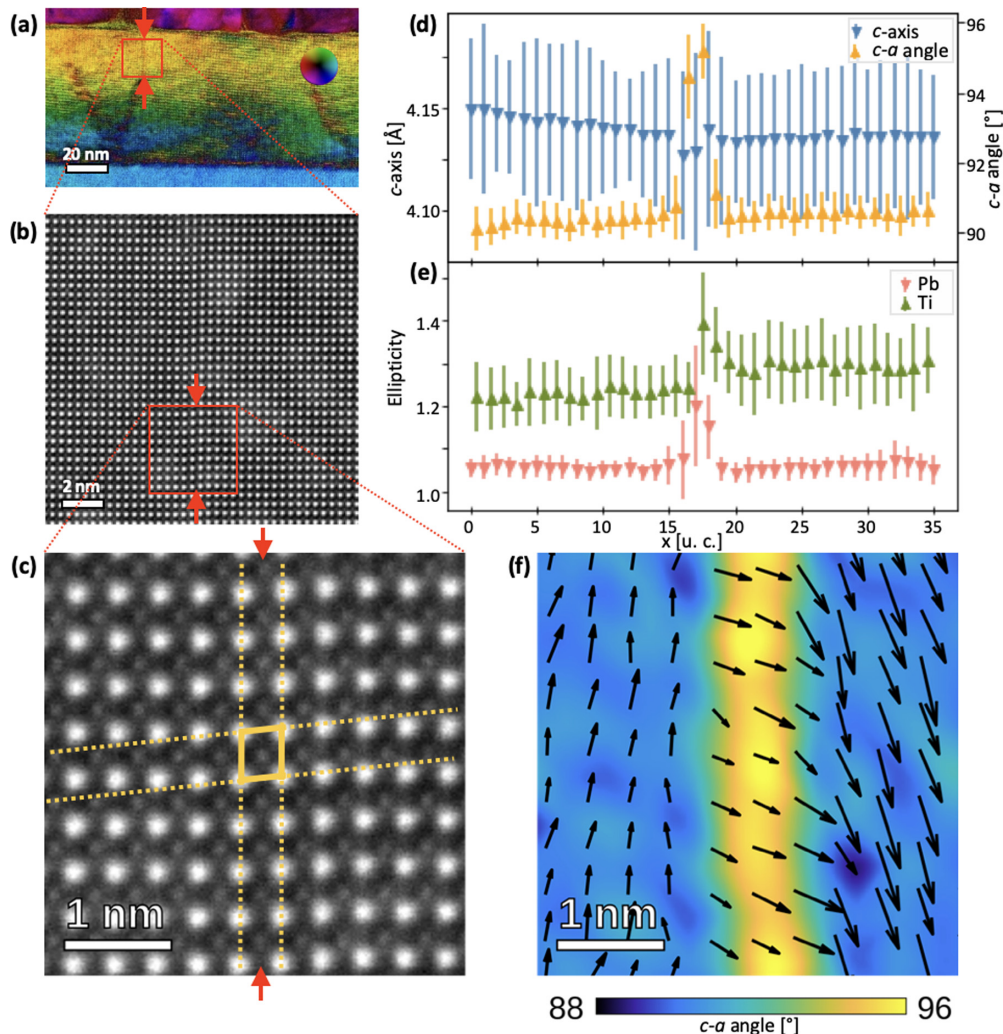
FIG. 3. Transmission electron microscopy and cross-section polarization mapping of intrinsic domain walls at room temperature. (a) Low-magnification differential phase contrast (DPC) TEM image of the sample, allowing visualization of the domain wall positions. (b) High-magnification HAADF-STEM image of the region indicated by the red box in (a). The domain wall is visible as a shift in the Pb lattice close to the center of the image (see main text). (c) Cropped version of the atomic resolution HAADF shown in (b). Here the Ti atom columns are readily visible, as well as the shift in the Pb lattice, inducing a sharp change in the c-a angle highlighted by the yellow dotted lines. The domain wall position is indicated by red arrows in (a)–(c). (d) c axis and c-a angle extracted from 2D Gaussian fits to the positions of the atomic columns in (b). The position of the domain wall is clearly visible as an increase in c-a angle. (e) Ellipticities of the Pb and Ti columns, caused by the projection of different positions of the atoms throughout the thickness of the lamella. The Ti ellipticity is higher throughout, consistent with the averaging over opposite polarization directions through the thickness of the lamella. (f) Reconstructed polarization map based on a three-Gaussian fit to the position of the Ti columns in (c) (see main text). The color scale indicates the interpolated c-a angle, which we use as a marker for the position of the domain wall. The arrows represent the polarization extracted from the Ti displacement, which follows a typical Néel pattern.

comparing with the image obtained by SHG on the same sample and at the same scale [Fig. 4(b)], we nonetheless observe regions of brighter and darker SHG contrast. This signal confirms the presence of an in-plane component of polarization. However, these contrast variations appear at much larger length scales than the individual nanoscale domains imaged by PFM. Indeed, radially averaged autocorrelation for each image reveals a characteristic pseudoperiod of approximately 800 nm for the SHG contrast variations, but only about 100 nm for the PFM images, corresponding directly to the domain structure (see Supplemental Material [38] Sec. S2 for details).

Nonetheless, when the microstructure of domains [Fig. 4(c)] and domain walls [Fig. 4(d)] in the PFM image is explicitly blurred to mimic the lower resolution and averaging effect of SHG, longer-range variations in density are clearly revealed. Radially averaged autocorrelation analysis of this resulting superstructure shows the same approximately 800 nm pseudoperiod as that of the intensity variations in the SHG image [Fig. 4(e)].

This superstructure in the domain density appears to be directly linked to the underlying defect landscape. To demonstrate this, we apply this radially averaged autocorrelation
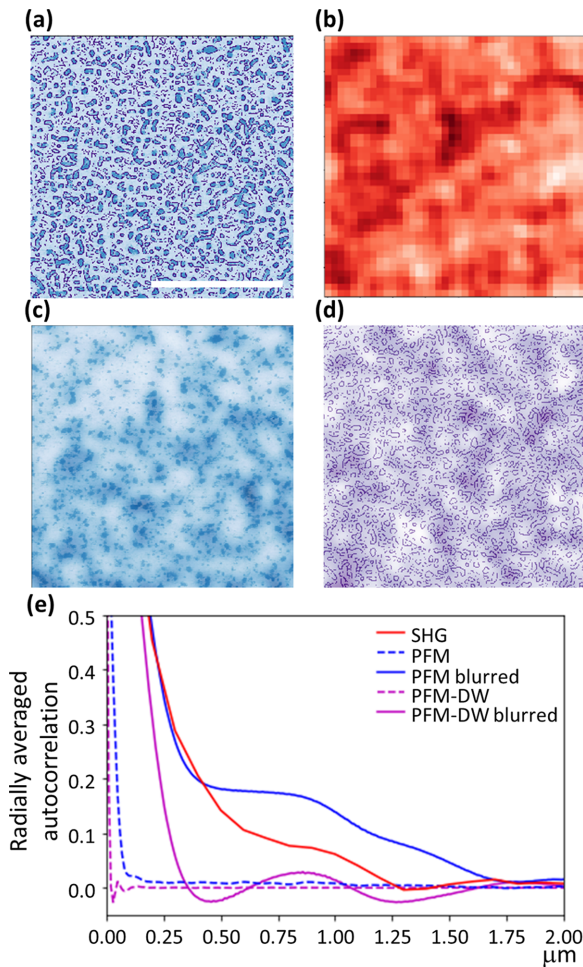
FIG. 4. Characteristic length scale of domain superstructure. (a) Vertical PFM phase image of the domain structure of the polydomain sample in blue (ranging from $0°$ to $180°$), with the edges detected using the Canny edge detection algorithm in purple. (b) SHG image of the same sample. The dark and bright contrast cannot be directly related to the domain pattern or to the domain edges. (c) and (d) Local density variations revealed by blurring applied on the vertical PFM phase image of the domains in (c) and on the domain wall structure (d). These domain density variations appear to closely match the variation observed in SHG intensity. All images are shown at the same scale, indicated by the 2-μm white scale bar in (a). (e) Radially averaged autocorrelation for the SHG image and both the domain and domain wall (DW) distributions obtained from the PFM phase image, and their superstructure obtained after blurring. While only very small structures are revealed in the raw PFM images, the superstructure in the density has the same pseudoperiod as the contrast variations found in the SHG image.

analysis to a simple Ising model simulation shown in Fig. 5(a), in which a disorder potential with a characteristic length scale ξ is added to the Ising Hamiltonian, and the resulting domain density fluctuations are blurred to reveal their superstructure, as for the experimental analysis (see Supplemental Material [38] Sec. S3 for details). As can be seen in Fig. 5(b), we find that the typical feature size extracted from radially averaged autocorrelation analysis exactly matches the characteristic length scale ξ of the disorder potential.

While the effect of strong, localized defects can be seen in, for example, the changes in roughness at domain walls [52], our observation of a characteristic length scale of 800 nm seems more compatible with variations of a collective background defect potential. This potential has been previously mapped out using spectroscopic techniques [47], recently further assisted by machine learning [53]. We note, moreover, that the key contributions to the disorder landscape do not appear to be variations of the surface morphology (see Supplemental Material [38] Fig. S10 for details). Our analysis therefore demonstrates that quantitative information on this defect potential—its characteristic length scale—can be obtained using noninvasive and nondestructive optical measurements, without the need to switch the intrinsic domains and thus modify the defect landscape of the film [39,54]. This method can be applied more generally, for example, to samples where the defect density has been engineered, to reveal the resulting change in domain density superstructure.

In summary, our complementary PFM, SHG, and TEM measurements demonstrate that both artificial and naturally occurring domain walls in PbTiO$_3$ thin films present components of Néel polarization at room temperature, possibly stabilized over the predicted Ising structure by defect segregation. Indeed, radially averaged autocorrelation analysis of domain density fluctuations reveals characteristic length scales which can be related to variations in the underlying disorder potential landscape. While it remains to be explored if and how such domain walls transition to a Bloch configuration at low temperature, our observations suggest potential utility in novel nanoelectronic applications, as Néel domain walls would be locally more likely to show increased electrical conductivity than their Ising counterparts (see Supplemental Material Sec. S4 for details).

The data that support the findings of this study are available at Yareta [55].

P.P. and S.C.-H. designed the experiment; C.W. and C.L. grew the samples and conducted the piezoresponse force microscopy; S.C.-H. carried out the second-harmonic generation microscopy in collaboration with K.D.D; A.B.N. performed the transmission electron microscopy and the atomic position fitting; C.W. carried out the autocorrelation analysis; I.G. performed the Monte Carlo simulations of the perturbed Ising model; C.W., C.L., A.B.N., and P.P. wrote the manuscript with contributions from all authors. All authors discussed the experimental results and models, commented on the manuscript, and agreed on its final version.
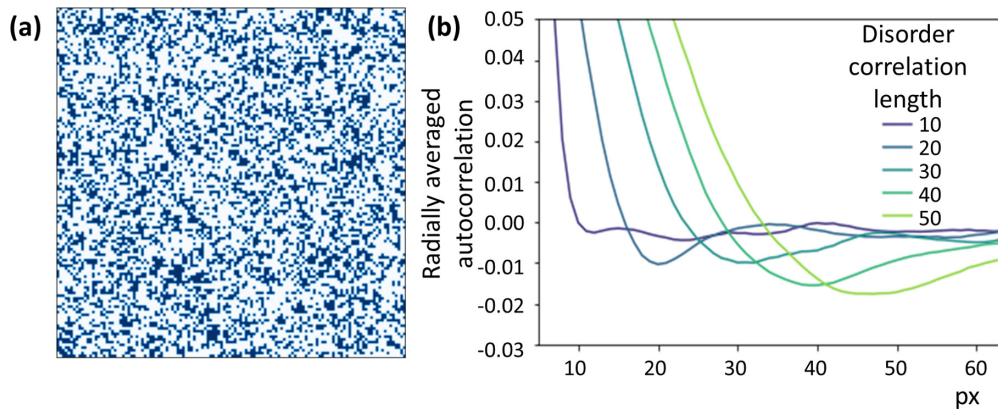
FIG. 5. Simulations of domain density variations demonstrating the importance of the disorder correlation length. Experimentally observed fluctuations of domain density were reproduced using an Ising system with a random disorder potential of characteristic length scale ξ. (a) Relaxed domain structure after randomly distributed up- and down-polarization regions, initially in equal proportion, were subjected to a random field disorder potential. (b) The radially averaged autocorrelation function of the domain superstructure, whose first minima, corresponding to the typical feature size, exactly match the disorder correlation length. Here, px, pixels.

[1] N. Setter, D. Damjanovic, L. Eng, G. Fox, S. Gevorgian, S. Hong, A. Kingon, H. Kohlstedt, N. Y. Park, G. B. Stephenson, I. Stolitchnov, A. K. Taganstev, D. V. Taylor, T. Yamada, and S. Streiffer, Ferroelectric thin films: Review of materials, properties, and applications, J. Appl. Phys. **100**, 051606 (2006).

[2] J. Seidel, L. W. Martin, Q. He, Q. Zhan, Y.-H. Chu, A. Rother, M. E. Hawkridge, P. Maksymovych, P. Yu, M. Gajek, N. Balke, S. V. Kalinin, S. Gemming, F. Wang, G. Catalan, J. F. Scott, N. A. Spaldin, J. Orenstein, and R. Ramesh, Conduction at domain walls in oxide multiferroics, Nat. Mater. **8**, 229 (2009).

[3] J. Guyonnet, I. Gaponenko, S. Gariglio, and P. Paruch, Conduction at domain walls in insulating $Pb(Zr_{0.2}Ti_{0.8})O_3$ thin films, Adv. Mater. **23**, 5377 (2011).

[4] M. Daraktchiev, G. Catalan, and J. F. Scott, Landau theory of domain wall magnetoelectricity, Phys. Rev. B **81**, 224118 (2010).

[5] G. Catalan, J. Seidel, R. Ramesh, and J. F. Scott, Domain wall nanoelectronics, Rev. Mod. Phys. **84**, 119 (2012).

[6] D. Meier, J. Seidel, A. Cano, K. Delaney, Y. Kumagai, M. Mostovoy, N. A. Spaldin, R. Ramesh, and M. Fiebig, Anisotropic conductance at improper ferroelectric domain walls, Nat. Mater. **11**, 284 (2012).

[7] P. Paruch and J. Guyonnet, Nanoscale studies of ferroelectric domain walls as pinned elastic interfaces, C. R. Phys. **14**, 667 (2013).

[8] J. R. Whyte, R. G. P. McQuaid, P. Sharma, C. Canalias, J. F. Scott, A. Gruverman, and J. M. Gregg, Ferroelectric domain wall injection, Adv. Mater. **26**, 293 (2014).

[9] L. J. McGilly, P. Yudin, L. Feigl, A. K. Tagantsev, and N. Setter, Controlling domain wall motion in ferroelectric thin films, Nat. Nanotechnol. **10**, 145 (2015).

[10] D. Lee, R. K. Behera, P. Wu, H. Xu, Y. L. Li, S. B. Sinnott, S. R. Phillpot, L. Q. Chen, and V. Gopalan, Mixed Bloch-Néel-Ising character of 180° ferroelectric domain walls, Phys. Rev. B **80**, 060102(R) (2009).

[11] P. Marton, I. Rychetsky, and J. Hlinka, Domain walls of ferroelectric $BaTiO_3$ within the Ginzburg-Landau-Devonshire phenomenological model, Phys. Rev. B **81**, 144125 (2010).

[12] V. Stepkova, P. Marton, and J. Hlinka, Stress-induced phase transition in ferroelectric domain walls of $BaTiO_3$, J. Phys.: Condens. Matter **24**, 212201 (2012).

[13] P. Marton, V. Stepkova, and J. Hlinka, Divergence of dielectric permittivity near phase transition within ferroelectric domain boundaries, Phase Transitions **86**, 103 (2013).

[14] Y.-J. Wang, Y.-L. Zhu, and X.-L. Ma, Chiral phase transition at 180° domain walls in ferroelectric $PbTiO_3$ driven by epitaxial compressive strains, J. Appl. Phys. **122**, 134104 (2017).

[15] J. C. Wojdeł and J. Íñiguez, Ferroelectric Transitions at Ferroelectric Domain Walls Found from First Principles, Phys. Rev. Lett. **112**, 247603 (2014).

[16] E. A. Eliseev, P. V. Yudin, S. V. Kalinin, N. Setter, A. K. Tagantsev, and A. N. Morozovska, Structural phase transitions and electronic phenomena at 180-degree domain walls in rhombohedral $BaTiO_3$, Phys. Rev. B **87**, 054111 (2013).

[17] X. K. Wei, C. L. Jia, T. Sluka, B. X. Wang, Z. G. Ye, and N. Setter, Néel-like domain walls in ferroelectric $Pb(Zr,Ti)O_3$ single crystals, Nat. Commun. **7**, 12385 (2016).

[18] G. De Luca, M. D. Rossell, J. Schaab, N. Viart, M. Fiebig, and M. Trassin, Domain wall architecture in tetragonal ferroelectric thin films, Adv. Mater. **29**, 1605145 (2017).

[19] S. Cherifi-Hertel, H. Bulou, R. Hertel, G. Taupier, K. D. H. Dorkenoo, C. Andreas, J. Guyonnet, I. Gaponenko, K. Gallo, and P. Paruch, Non-Ising and chiral ferroelectric domain walls revealed by nonlinear optical microscopy, Nat. Commun. **8**, 15768 (2017).

[20] A. K. Yadav, C. T. Nelson, S. L. Hsu, Z. Hong, J. D. Clarkson, C. M. Schlepütz, A. R. Damodaran, P. Shafer, E. Arenholz, L. R. Dedon, D. Chen, A. Vishwanath, A. M. Minor, L. Q. Chen, J. F. Scott, L. W. Martin, and R. Ramesh, Observation of polar vortices in oxide superlattices, Nature (London) **530**, 198 (2016).

[21] V. A. Stoica, N. Laanait, C. Dai, Z. Hong, Y. Yuan, Z. Zhang, S. Lei, M. R. McCarter, A. Yadav, A. R. Damodaran, S. Das, G. A. Stone, J. Karapetrova, D. A. Walko, X. Zhang, L. W. Martin, R. Ramesh, L.-Q. Chen, H. Wen, V. Gopalan *et al.*, Optical creation of a supercrystal with three-dimensional nanoscale periodicity, Nat. Mater. **18**, 377 (2019).

[22] M. Hadjimichael, Ferroelectric domains in lead titanate heterostructures, PhD. thesis, University College London, 2019.

[23] M. Hadjimichael, Y. Li, E. Zatterin, G. A. Chahine, M. Conroy, K. Moore, E. N. Connell, P. Ondrejkovic, P. Marton, J. Hlinka, U. Bangert, S. Leake, and P. Zubko, Metal-ferroelectric supercrystals with periodically curved metallic layers, Nat. Mater. **20**, 495 (2021).

[24] M. A. P. Gonçalves, C. Escorihuela-Sayalero, P. Garca-Fernández, J. Junquera, and J. Íñiguez, Theoretical guidelines to create and tune electric skyrmion bubbles, Sci. Adv. **5**, eaau7023 (2019).

[25] S. Das, Y. L. Tang, Z. Hong, M. A. P. Gonçalves, M. R. McCarter, C. Klewe, K. X. Nguyen, F. Gómez-Ortiz, P. Shafer, E. Arenholz, V. A. Stoica, S.-L. Hsu, B. Wang, C. Ophus, J. F. Liu, C. T. Nelson, S. Saremi, B. Prasad, A. B. Mei, D. G. Schlom, J. Íñiguez, P. García-Fernández, D. A. Muller, L. Q. Chen *et al.*, Observation of room-temperature polar skyrmions, Nature (London) **568**, 368 (2019).

[26] R. K. Behera, C.-W. Lee, D. Lee, A. N. Morozovska, S. B. Sinnott, A. Asthagiri, V. Gopalan, and S. R. Phillpot, Structure and energetics of 180° domain walls in PbTiO$_3$ by density functional theory, J. Phys.: Condens. Matter **23**, 175902 (2011).

[27] Q. Zhang, L. Xie, G. Liu, S. Prokhorenko, Y. Nahas, X. Pan, L. Bellaiche, A. Gruverman, and N. Valanoor, Nanoscale bubble domains and topological transitions in ultrathin ferroelectric films, Adv. Mater. **29**, 1702375 (2017).

[28] C. Lichtensteiger, S. Fernandez-Pena, C. Weymann, P. Zubko, and J.-M. Triscone, Tuning of the depolarization field and nanodomain structure in ferroelectric thin films, Nano Lett. **14**, 4205 (2014).

[29] C. Lichtensteiger, C. Weymann, S. Fernandez-Pena, P. Paruch, and J.-M. Triscone, Built-in voltage in thin ferroelectric PbTiO$_3$ films: The effect of electrostatic boundary conditions, New J. Phys. **18**, 043030 (2016).

[30] C. Weymann, C. Lichtensteiger, S. Fernandez-Peña, A. B. Naden, L. R. Dedon, L. W. Martin, J.-M. Triscone, and P. Paruch, Full control of polarization in ferroelectric thin films using growth temperature to modulate defects, Adv. Electron. Mater. **6**, 2000852 (2020).

[31] P. Aguado-Puente and J. Junquera, Structural and energetic properties of domains in PbTiO$_3$/SrTiO$_3$ superlattices from first principles, Phys. Rev. B **85**, 184105 (2012).

[32] T. Rojac, A. Bencan, G. Drazic, N. Sakamoto, H. Ursic, B. Jancar, G. Tavcar, M. Makarovic, J. Walker, B. Malic, and D. Damjanovic, Domain-wall conduction in ferroelectric BiFeO$_3$ controlled by accumulation of charged defects, Nat. Mater. **16**, 322 (2017).

[33] G. Shirane, J. D. Axe, J. Harada, and J. P. Remeika, Soft ferroelectric modes in lead titanate, Phys. Rev. B **2**, 155 (1970).

[34] A. B. Yankovich, B. Berkels, W. Dahmen, P. Binev, S. I. Sanchez, S. A. Bradley, A. Li, I. Szlufarska, and P. M. Voyles, Picometre-precision analysis of scanning transmission electron microscopy images of platinum nanocatalysts, Nat. Commun. **5**, 4155 (2014).

[35] W. Y. Wang, Y. L. Tang, Y. L. Zhu, Y. B. Xu, Y. Liu, Y. J. Wang, S. Jagadeesh, and X. L. Ma, Atomic level 1D structural modulations at the negatively charged domain walls in BiFeO$_3$ films, Adv. Mater. Int. **2**, 1500024 (2015).

[36] A. Bencan, E. Oveisi, S. Hashemizadeh, V. K. Veerapandiyan, T. Hoshina, T. Rojac, M. Deluca, G. Drazic, and D. Damjanovic, Atomic scale symmetry and polar nanoclusters in the paraelectric phase of ferroelectric materials, Nat. Commun. **12**, 3509 (2021).

[37] D. Mukherjee, L. Miao, G. Stone, and N. Alem, mpfit: A robust method for fitting atomic resolution images with multiple Gaussian peaks, Adv. Struct. Chem. Imaging **6**, 1 (2020).

[38] See Supplemental Material at http://link.aps.org/supplemental/10.1103/PhysRevB.106.L241404 for further information about scanning transmission electron microscopy data acquisition and analysis, radially averaged autocorrelation analysis, Ising model with disorder, non-Ising structure and conductive properties of ferroelectric domain walls, second-harmonic generation, thin-film growth, and scanning probe microscopy. See also Refs. [3,10,12,15,18–20,23–25,30,42–46,51,56–66] therein.

[39] S. V. Kalinin, S. Jesse, A. Tselev, A. P. Baddorf, and N. Balke, The role of electrochemical phenomena in scanning probe microscopy of ferroelectric thin films, ACS Nano **5**, 5683 (2011).

[40] U. Acevedo-Salas, B. Croes, Y. Zhang, O. Cregut, K. D. Dorkenoo, B. Kirbus, E. Singh, H. Beccard, M. Rüsing, L. M. Eng, E. A. Eliseev, A. N. Morozovska, and S. Cherifi-Hertel, Impact of 3D curvature on the polarization orientation in non-Ising domain walls, arXiv:2207.01307.

[41] C. L. Jia, K. W. Urban, M. Alexe, D. Hesse, and I. Vrejoiu, Direct observation of continuous electric dipole rotation in flux-closure domains in ferroelectric Pb(Zr,Ti)O$_3$, Science **331**, 1420 (2011).

[42] A. N. Morozovska, E. A. Eliseev, M. D. Glinchuk, L. Q. Chen, S. V. Kalinin, and V. Gopalan, Impact of free charges on polarization and pyroelectricity in antiferrodistortive structures and surfaces induced by a flexoelectric effect, Ferroelectrics **438**, 32 (2012).

[43] E. A. Eliseev, A. N. Morozovska, G. S. Svechnikov, P. Maksymovych, and S. V. Kalinin, Domain wall conduction in multiaxial ferroelectrics, Phys. Rev. B **85**, 045312 (2012).

[44] L. Feigl, P. Yudin, I. Stolichnov, T. Sluka, K. Shapovalov, M. Mtebwa, C. S. Sandu, X.-K. Wei, A. K. Tagantsev, and N. Setter, Controlled stripes of ultrafine ferroelectric domains, Nat. Commun. **5**, 4677 (2014).

[45] I. Stolichnov, L. Feigl, L. J. McGilly, T. Sluka, X. K. Wei, E. Colla, A. Crassous, K. Shapovalov, P. Yudin, A. K. Tagantsev, and N. Setter, Bent ferroelectric domain walls as reconfigurable metallic-like channels, Nano Lett. **15**, 8049 (2015).

[46] Y. Cao, L. Q. Chen, and S. V. Kalinin, Role of flexoelectric coupling in polarization rotations at the a-c domain walls in ferroelectric perovskites, Appl. Phys. Lett. **110**, 202903 (2017).

[47] S. Jesse, B. J. Rodriguez, S. Choudhury, A. P. Baddorf, I. Vrejoiu, D. Hesse, M. Alexe, E. A. Eliseev, A. N. Morozovska, J. Zhang, L.-Q. Chen, and S. V. Kalinin, Direct imaging of the spatial and energy distribution of nucleation centres in ferroelectric materials, Nat. Mater. **7**, 209 (2008).

[48] C. Blaser and P. Paruch, Minimum domain size and stability in carbon nanotube-ferroelectric devices, Appl. Phys. Lett. **101**, 142906 (2012).

[49] P. Tueckmantel, I. Gaponenko, N. Caballero, J. C. Agar, L. W. Martin, T. Giamarchi, and P. Paruch, Local Probe Comparison of Ferroelectric Switching Event Statistics in the Creep and Depinning Regimes in Pb(Zr$_{0.2}$Ti$_{0.8}$)O$_3$ Thin Films, Phys. Rev. Lett. **126**, 117601 (2021).

[50] S. Farokhipoor and B. Noheda, Conduction through 71° Domain Walls in BiFeO$_3$ Thin Films, Phys. Rev. Lett. **107**, 127601 (2011).

[51] J. Seidel, P. Maksymovych, Y. Batra, A. Katan, S.-Y. Yang, Q. He, A. P. Baddorf, S. V. Kalinin, C.-H. Yang, J.-C. Yang, Y.-H. Chu, E. K. H. Salje, H. Wormeester, M. Salmeron, and R. Ramesh, Domain Wall Conductivity in La-Doped BiFeO$_3$, Phys. Rev. Lett. **105**, 197603 (2010).

[52] J. Guyonnet, Growing up at the nanoscale: Studies of ferroelectric domain wall functionalities, roughening, and dynamic properties by atomic force microscopy, Ph.D. thesis, Université de Genève, 2013.

[53] J. C. Agar, Y. Cao, B. Naul, S. Pandya, S. van der Walt, A. I. Luo, J. T. Maher, N. Balke, S. Jesse, S. V. Kalinin, R. K. Vasudevan, and L. W. Martin, Machine detection of enhanced electromechanical energy conversion in PbZr$_{0.2}$Ti$_{0.8}$O$_3$ thin films, Adv. Mater. **30**, 1800701 (2018).

[54] N. Domingo, I. Gaponenko, K. Cordero-Edwards, N. Stucki, V. Pérez-Dieste, C. Escudero, E. Pach, A. Verdaguer, and P. Paruch, Surface charged species and electrochemistry of ferroelectric thin films, Nanoscale **11**, 17920 (2019).

[55] https://doi.org/10.26037/yaretateri72ux7fhqlgj435imm2ubiq.

[56] M. Nord, P. E. Vullum, I. MacLaren, T. Tybell, and R. Holmestad, Atomap: A new software tool for the automated analysis of atomic resolution images using two-dimensional Gaussian fitting, Adv. Struct. Chem. Imaging **3**, 9 (2017).

[57] E. Bousquet, First-principles study of ferroelectric oxide nanostructures, Ph.D. thesis, Université de Liège, 2008.

[58] I. Gaponenko, P. Tückmantel, J. Karthik, L. W. Martin, and P. Paruch, Towards reversible control of domain wall conduction in Pb(Zr$_{0.2}$Ti$_{0.8}$)O$_3$ thin films, Appl. Phys. Lett. **106**, 162902 (2015).

[59] C. Weymann, C. Lichtensteiger, S. Fernandez-Peña, K. Cordero-Edwards, and P. Paruch, Improved thin film growth using slow kinetics intermittent sputtering, Appl. Surf. Sci. **516**, 146077 (2020).

[60] S. Farokhipoor and B. Noheda, Local conductivity and the role of vacancies around twin walls of (001)-BiFeO$_3$ thin films, J. Appl. Phys. **112**, 052003 (2012).

[61] S. Cherifi-Hertel, C. Voulot, U. Acevedo-Salas, Y. Zhang, O. Crégut, K. D. Dorkenoo, and R. Hertel, Shedding light on non-Ising polar domain walls: Insight from second harmonic generation microscopy and polarimetry analysis, J. Appl. Phys. **129**, 081101 (2021).

[62] P. Maksymovych, A. N. Morozovska, P. Yu, E. A. Eliseev, Y. H. Chu, R. Ramesh, A. P. Baddorf, and S. V. Kalinin, Tunable metallic conductance in ferroelectric nanodomains, Nano Lett. **12**, 209 (2012).

[63] Z. Hong, S. Das, C. Nelson, A. K. Yadav, Y. Wu, J. Junquera, L.-Q. Chen, L. W. Martin, and R. Ramesh, Vortex domain walls in ferroelectrics, Nano Lett. **21**, 3533 (2021).

[64] B. J. Rodriguez, C. Callahan, S. V. Kalinin, and R. Proksch, Dual-frequency resonance-tracking atomic force microscopy, Nanotechnology **18**, 475504 (2007).

[65] P. Ghosez, J.-P. Michenaud, and X. Gonze, Dynamical atomic charges: The case of ABO$_3$ compounds, Phys. Rev. B **58**, 6224 (1998).

[66] J. B. Neaton, C. Ederer, U. V. Waghmare, N. A. Spaldin, and K. M. Rabe, First-principles study of spontaneous polarization in multiferroic BiFeO$_3$, Phys. Rev. B **71**, 014113 (2005).